solids

MDPI

Article

Finite Element Diagnosis and Material-Based Redesign of Dosing Pump Plungers: A Case Study of Premature Failure with Galling Damage

David de Armas Yanes [1], Christian Leandro Rodríguez Valladares [2], Luis Angel Iturralde Carrera [3,*], Yoisdel Castillo Alvarez [4,*], Carlos D. Constantino-Robles [3] and Juvenal Rodríguez-Reséndiz [3]

[1] Department of Mechanical Engineering, Faculty of Engineering, Universidad de Cienfuegos "Carlos Rafael Rodríguez", Cienfuegos 59430, Cuba
[2] Department of Electrical Power Engineering, Faculty of Electrical Engineering, Universidad Central "Marta Abreu" de Las Villas, Santa Clara 54830, Cuba
[3] Facultad de Ingeniería, Universidad Autónoma de Querétaro, Santiago de Querétaro 76010, Mexico
[4] Departamento de Ingeniería Mecánica, Universidad Tecnológica del Peru, Lima 15046, Peru
* Correspondence: liturralde28@alumnos.uaq.mx (L.A.I.C.); c19773@utp.edu.pe (Y.C.A.)

Abstract

The premature failure (service life ≈ 4 months) of AISI 321 steel plungers due to galling in critical dosing pumps at a thermoelectric power plant significantly compromises system reliability. This study identifies the root cause of this recurring failure and develops a robust engineering solution. Finite element analysis (FEA) was employed to diagnose the original component and numerically validate a redesign using 17-4 PH H900 steel. Additionally, economic viability was assessed through a Life-Cycle Cost (LCC) analysis. The FEA revealed a severe stress concentration where the original design operated at 97.3% of its yield strength, with a critical safety factor of 1.03. This finding suggested that the structural deficiency may have indirectly contributed to the observed galling damage by compromising the contact conditions in the guiding elements. This coupling is proposed as a mechanistic hypothesis, not as an experimentally validated tribological mechanism. The redesigned plunger achieved a safety factor of 5.74, representing a 457% increase in the structural safety margin. Furthermore, the LCC analysis demonstrated the economic superiority of locally manufacturing the improved component rather than importing the original spare part. Ultimately, the proposed solution eliminates the failure's root cause, proving to be structurally robust and economically viable. The methodology presented offers a transferable framework for diagnosing and redesigning critical industrial components.

Keywords: dosing pump plunger; finite element analysis (FEA); galling; tribo-mechanical failure; component redesign

Check for updates

Academic Editors: Adesola S. Ademiloye and John D. Clayton

Received: 8 August 2026
Revised: 19 September 2026
Accepted: 30 September 2026
Published: 5 November 2026

Copyright: © 2026 by the authors. Licensee MDPI, Basel, Switzerland. This article is an open access article distributed under the terms and conditions of the Creative Commons Attribution (CC BY) license.

1. Introduction

The operational reliability of thermoelectric power plants is a fundamental pillar for the stability of global energy grids. Within these complex systems, the integrity of the water-steam cycle is of utmost importance, as failures in chemical treatment can induce corrosion and scaling phenomena that compromise boiler efficiency and safety [1,2]. The precise dosing of chemical additives, such as phosphates, is a critical protection strategy to maintain boiler water pH and mitigate the effects of hardness, particularly in coastal plants susceptible to condensate contamination by seawater. The failure of these dosing

systems can nullify an essential chemical protection barrier, leading to unscheduled plant shutdowns with significant economic and operational repercussions [3–5].

AISI 321 is a titanium-stabilized austenitic stainless steel widely used in industrial components requiring good corrosion resistance, oxidation resistance, and mechanical stability at elevated temperatures. These characteristics make it an attractive material for equipment operating in chemically aggressive environments. However, despite its favorable corrosion performance, AISI 321 exhibits comparatively limited surface hardness and wear resistance under severe sliding-contact conditions [6–8]. Previous tribological studies have reported adhesive wear, plastic deformation, and material removal in untreated AISI 321, demonstrating that adequate corrosion resistance does not necessarily imply satisfactory tribological performance [5,9–11].

Among the degradation mechanisms affecting austenitic stainless steels, adhesive wear and galling are particularly important in components subjected to reciprocating or sliding contact. Galling involves localized adhesion between interacting metallic surfaces followed by severe plastic deformation, material transfer, and progressive material removal. Its initiation and severity are strongly affected by contact pressure, sliding distance, surface hardness, roughness, lubrication conditions, and the mechanical characteristics of the interacting materials [12–15]. Disruption of the passive surface layer under highly localized contact conditions may facilitate direct metal-to-metal interaction, promoting adhesion and subsequent material tear-out. In precision components, progressive galling can therefore degrade dimensional tolerances and ultimately compromise sealing and functional performance [4,16,17].

Different strategies have been investigated to mitigate the tribological limitations of austenitic stainless steels, including thermochemical treatments, surface coatings, laser texturing, lubrication optimization, and modifications intended to increase surface hardness [18–20]. In AISI 321, for example, surface modification through aluminizing has been shown to substantially improve hardness and wear resistance [11]. Although these approaches can enhance local tribological performance, most primarily focus on the material or contact surface [21]. Comparatively less attention has been devoted to the possible interaction between the global structural response of a component and the local contact conditions that govern adhesive wear and galling.

The present study originates from a recurring failure observed in the trisodium phosphate dosing pumps of the “Carlos Manuel de Céspedes” Thermoelectric Power Plant in Cienfuegos, Cuba. The original AISI 321 stainless steel plungers exhibited an operational life of only approximately four months. Rather than macroscopic fracture, the components developed severe surface degradation consistent with galling, progressively compromising dimensional tolerances and producing internal leakage and loss of dosing capacity. The conventional maintenance strategy consisted of periodically replacing the failed plunger with an identical imported component, thereby perpetuating the failure cycle without addressing its underlying cause and increasing both maintenance costs and vulnerability of the boiler-protection system.

Based on the observed failure and the known tribological limitations of austenitic stainless steels, this study hypothesizes that the premature degradation of the plunger cannot be attributed exclusively to surface wear. Instead, an unfavorable structural stress state may act as an indirect contributor to galling by progressively degrading the contact conditions between the plunger and its guiding elements. Accordingly, the novelty of this work lies in treating the failure as a coupled tribo-mechanical problem and integrating structural diagnosis, material selection, manufacturing feasibility, and economic assessment within a single engineering framework.

Therefore, the objectives of this study are (1) to perform a diagnostic finite element analysis (FEA) of the original AISI 321 plunger to assess its structural integrity under maximum operating conditions; (2) to redesign and numerically validate the component using precipitation-hardening 17-4 PH stainless steel in the H900 condition; (3) to define a feasible manufacturing route for local production of the redesigned component; and (4) to evaluate the economic viability of the proposed solution through a Life-Cycle Cost (LCC) analysis. Finite element analysis has been widely used in forensic engineering and redesign of industrial components, including shafts, valve stems, pump elements, and reciprocating parts, to identify stress concentrations, evaluate safety margins, and support material or geometric changes [22,23]. In this context, the present work combines FEA with a materials-based redesign and a Life-Cycle Cost analysis for a critical dosing pump plunger. The objective of this study is to diagnose the premature failure of an AISI 321 dosing pump plunger, redesign it using 17-4 PH H900 stainless steel, validate the redesign by comparative FEA under identical operating conditions, define a feasible local manufacturing route, and evaluate its economic viability through LCC analysis.

2. Materials and Methods

To further contextualize the present study within the current research landscape, a bibliometric keyword co-occurrence analysis was performed using scientific records retrieved from the Scopus database and visualized with VOSviewer 1.6.21 (Figure 1). The resulting network reveals finite element method as one of the most prominent and highly interconnected concepts, establishing strong relationships with terms associated with deformation, friction, wear, wear resistance, mechanical failure, failure mechanisms, residual stresses, and different metallic alloys. Several additional research domains, including high-strength steels, plastic deformation, fatigue crack propagation, coatings, and numerical simulation, are also closely connected within the network. This structure highlights the inherently multidisciplinary character of contemporary failure analysis, where computational mechanics, materials engineering, and tribology increasingly converge to explain the degradation and reliability of engineering components. In this context, the present work is positioned at the intersection of these research areas by combining finite element analysis with tribological failure interpretation and material-based redesign of a critical dosing pump plunger.

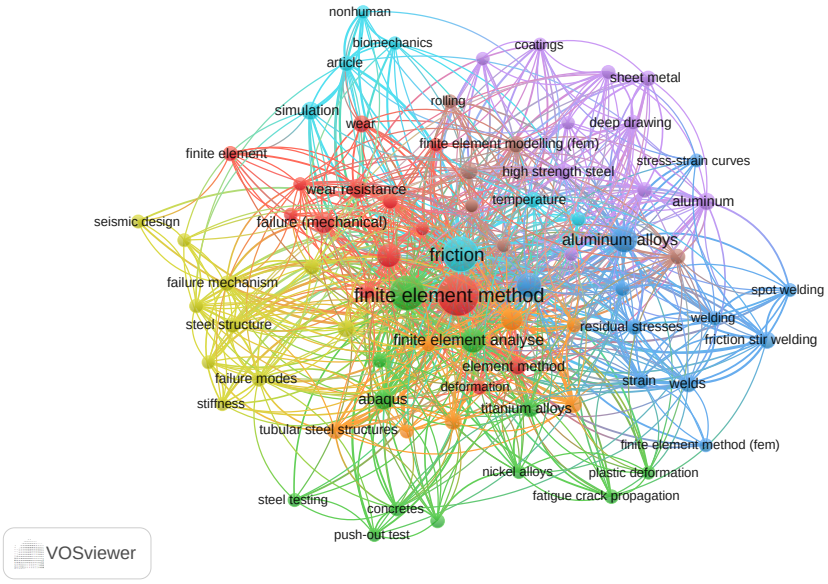


Figure 1. Bibliometric network of keyword co-occurrence in research related to finite element analysis, mechanical failure, tribology, and metallic materials.

The present research was systematically structured into three sequential phases to guarantee an exhaustive analysis: (1) a diagnostic analysis of the original component to identify the root cause of the premature failure, (2) the redesign and numerical validation of an improved component, and (3) the definition of a robust and repeatable manufacturing technology for the proposed solution. This integrated approach connects theoretical analysis with practical implementation, ensuring the viability of the final design.

2.1. Analysis of the Failed Component and Problem Definition

The starting point of this investigation was the analysis of an AISI 321 stainless steel plunger, removed from service in a dosing pump at the "Carlos Manuel de Céspedes" Thermoelectric Power Plant after approximately four months of operation. Figure 2 shows both the pump assembly and a detail of the failed component. Severe surface wear is observed on the working diameter of the plunger, characteristic of the galling phenomenon. This recurring failure defined the problem to be solved: determining the root cause of the accelerated degradation and proposing a robust engineering solution.

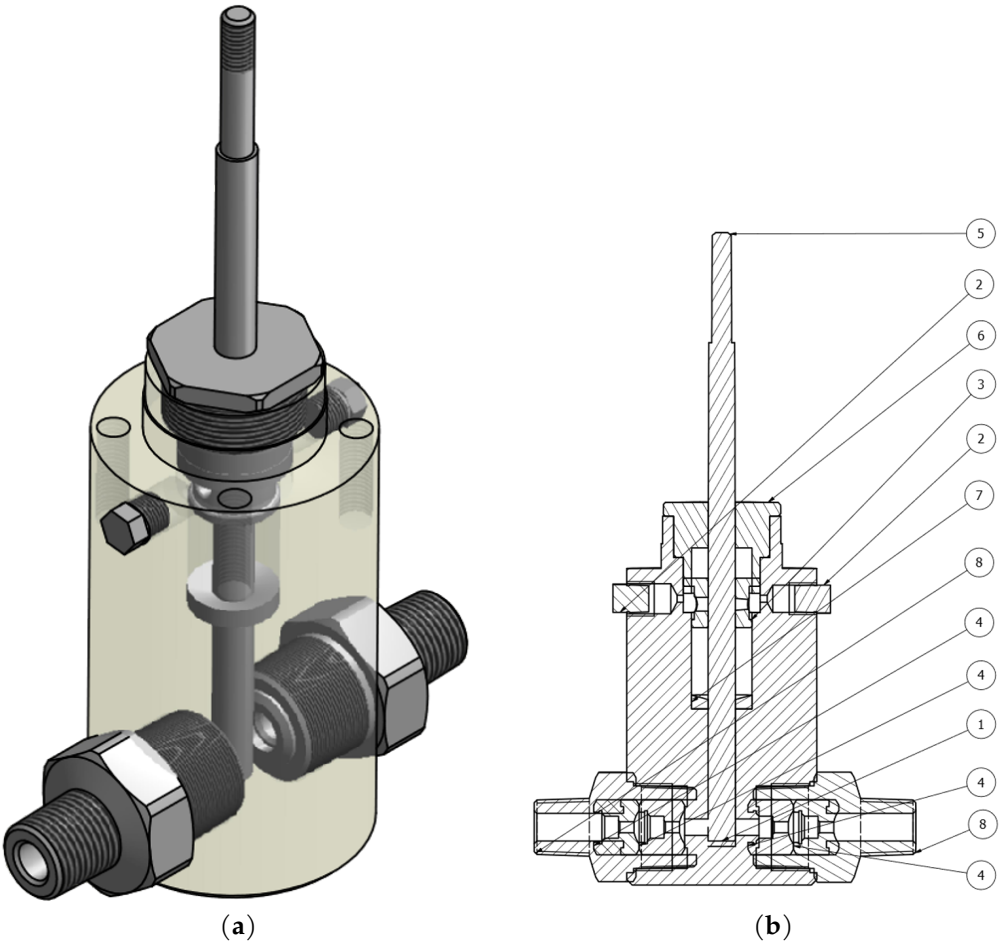


Figure 2. Dosing pump configuration. (**a**) 3D isometric view with a semi-transparent body to show the assembly context. (**b**) Cross-section detailing the internal components. The part legend is as follows: (1) Pump Body, (2) Plug, (3) Bushing, (4) Check Valve Body, (5) Plunger (Object of Study), (6) Packing Gland, (7) Packing Support, (8) Check Valve Support. The galling failure occurs at the tribological interface between the Plunger (5) and the guiding and sealing components (3, 6, and 7).

The main technical specifications and operating conditions of the dosing pump are summarized in Table 1.

Table 1. Pump specifications and operating conditions.

Parameter	Value
Pump manufacturer/model	LEWA GmbH, LEWA ecodos LDC1-M21S-K10/SST-E1
Application	Phosphate dosing in a 158 MW thermoelectric unit
Pump type	Positive displacement plunger pump
Nominal discharge pressure	200 bar (g)
Maximum discharge pressure	250 bar (g) (25 MPa)
Suction pressure	0.2 bar (g), minimum $NPSH_a$
Nominal flow	8 L/h
Maximum flow	~11.3 L/h
Plunger diameter	10 mm
Stroke	max. 20 mm
Strokes per minute	120–150 SPM
Operation regime	Continuous 24/7, 100% redundancy
Fluid	8% *w*/*v* Na_3PO_4 in demineralized water
pH	12.0–12.8
Fluid temperature	20–45 °C
Density	~1.07 kg/L at 25 °C
Viscosity	~1.2 cP at 25 °C
Head material	AISI 316L
Plunger material	X18H10T/AISI 321
Sealing/packing/guide counterface	Austenitic stainless steel (plant records report AISI 316L packing/guide components)
Motor	0.25 kW, 440 VAC/60 Hz, three-phase, TEFC, IP55, insulation class F

The pump operates continuously at ambient temperature (approximately 30 °C) in a coastal environment. The dosing flow is adjusted according to boiler water chemistry requirements, and the plunger is subjected to cyclic loading at 120–150 strokes per minute. Pressure transients up to the maximum discharge pressure of 25 MPa may occur during startup and shutdown sequences. The pumped fluid is a trisodium phosphate solution at ambient temperature. Figure 3 shows the failed plunger and the observed galling damage on the working diameter.



(**a**) (**b**)

Figure 3. Failed AISI 321 plunger. (**a**) Pump head during maintenance. (**b**) Galling damage on the working diameter.

2.2. Diagnostic Analysis of the Original Plunger (AISI 321)

The primary objective of this phase was to computationally investigate the hypothesis that the observed surface degradation (galling) was accelerated by an underlying structural deficiency, rather than being a purely tribological phenomenon. Finite element analysis (FEA) was employed to simulate the mechanical response of the plunger under maximum operational loads. The object of this study is the plunger of a high-pressure dosing pump, whose assembly and key components are shown in Figure 2. A high-fidelity three-dimensional CAD model of the original plunger was generated using Autodesk Inventor Professional 2025 [24]. The technical drawing of the original plunger, including its principal dimensions, tolerances, fits, and surface finish requirements, is presented in Figure 4. To accurately apply the boundary conditions that replicate physical constraints, the main cylindrical surface (working surface) was logically divided using the Split tool to isolate the contact areas with the guides. This procedure isolated discrete surface areas corresponding to the contact zones with the pump's guiding elements, allowing for a more precise simulation of the support conditions. The material assigned to the model was AISI 321 stainless steel in its annealed condition, reflecting the state of the original component. The key mechanical proper-ties used for the simulation were a yield strength (Sy) of 205 MPa, a Young's modulus (E) of 193 GPa, and a Poisson's ratio (v) of 0.29 [25]. The chemical composition and applicable standards for the original and proposed materials are given in Table 2. The plunger is geometrically axisymmetric, but the loading and support conditions are not perfectly symmetric because the guiding surfaces act only on discrete contact zones. Therefore, a full 3D model was used instead of a 2D axisymmetric simplification. The same geometry, mesh, and constitutive model (linear-elastic and isotropic) were used for both the original AISI 321 plunger and the redesigned 17-4 PH H900 plunger. Only the material properties were changed: yield strength, Young's modulus, and Poisson's ratio. Manufacturing-induced effects such as residual stresses, dimensional tolerances, and surface roughness were not explicitly included in the finite element model. These factors were considered outside the scope of the structural diagnosis, which focused on the nominal stress state under maximum operating pressure. Their potential influence on the contact conditions is acknowledged as a limitation of the present analysis. These properties were obtained from the consolidated literature in materials science [26]. A Static Structural Analysis was configured to evaluate the stress, displacement, and safety factor distributions in the plunger. This type of analysis was selected since the pump operates cyclically but at a low frequency, allowing the stress state at maximum pressure to be modeled as a worst-case quasi-static scenario. This approach is sufficient to determine if the component operates near its plastic deformation threshold.

Table 2. Chemical composition and applicable standards (wt.%).

Material	Standard	C	Si	Mn	P	S	Cr	Ni	Ti	Cu	Nb+Ta
AISI 321/X18H10T	GOST 5632; AISI 321; UNS S32100; EN 1.4541	≤0.08	≤1.00	≤2.00	≤0.045	≤0.030	17.0–19.0	9.0–12.0	≥5(C + N); ≤0.70	–	–
17-4 PH	ASTM A564; UNS S17400; AMS 5643	≤0.07	≤1.00	≤1.00	≤0.040	≤0.030	15.0–17.5	3.0–5.0	–	3.0–5.0	0.15–0.45

Boundary Conditions: To simulate in-service constraints, the following boundary conditions were applied. A Fixed constraint was assigned to the threaded section, which connects the plunger to the pump actuator, restricting all six degrees of freedom (three translational and three rotational) to model a rigid connection. A frictionless support was assigned to the previously defined guiding surfaces. This condition prevents translation

normal to the surface but allows free tangential movement, effectively simulating the behavior of a well-lubricated guide bushing and isolating the structural response to the main axial load. Loading: A pressure load of 25 MPa was applied uniformly over the front working face of the plunger [27]. This value corresponds to the maximum specified operating pressure for the dosing pump system, according to the manufacturer's technical data. Meshing Strategy: The solid model was discretized using second-order (10-node) tetrahedral elements, which are suitable for capturing stress gradients in complex geometries. Mesh quality was verified to ensure result convergence, with localized refinement in high-stress concentration regions, such as the fillet radius at the base of the working diameter. The final mesh, identical for both analyses, was generated with an average element size of 0.28 mm, resulting in a total of 768,127 elements and 1,093,261 nodes. The theoretical foundation of the finite element method employed in this study is well-established in the computational mechanics literature [28]. Manufacturing-induced effects such as residual stresses, dimensional tolerances, and surface roughness were not explicitly included in the finite element model. These factors were considered outside the scope of the structural diagnosis, which focused on the nominal stress state under maximum operating pressure. Their potential influence on the contact conditions is acknowledged as a limitation of the present analysis.

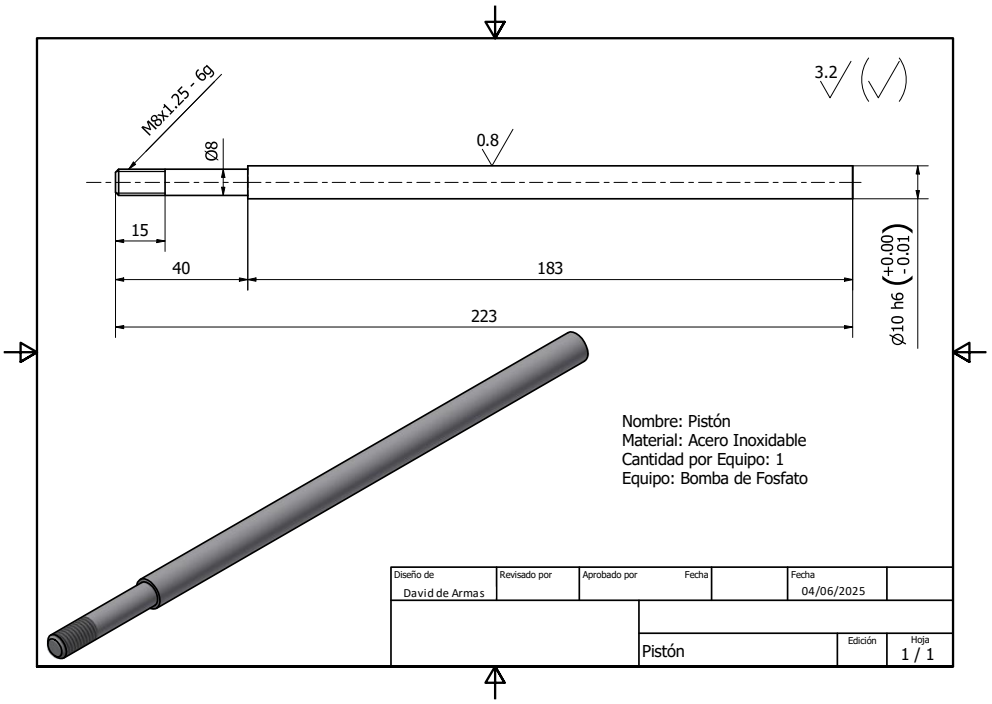


Figure 4. Technical drawing of original plunger. Dimensions are in millimeters.

2.3. Redesign and Numerical Validation of the Proposed Plunger (17-4 PH H900)

Following the diagnostic phase, a new plunger was designed using a high-er-performance material. Subsequently, a comparative FEA was conducted to quantitatively validate the performance improvement of the proposed solution under identical operating conditions. The material selected for the redesigned plunger was the precipitation-hardening stainless steel 17-4 PH. This alloy was chosen for its exceptional combination of high tensile strength, high hardness, and corrosion resistance—characteristics that directly address the identified failure mechanisms. The component was specified in the H900 heat-treatment condition, which optimizes strength and hardness. The mechanical properties assigned for the simulation were a yield strength (Sy) of 1170 MPa, a Young's modulus (E) of 196 GPa, and a Poisson's ratio (ν) of 0.25. 17-4 PH is a martensitic

precipitation-hardening stainless steel. The H900 designation refers to an aging treatment at 482 °C (900 °F) for 1 h followed by air cooling, applied after solution annealing (Condition A). This treatment produces a fine dispersion of copper-rich precipitates in a martensitic matrix, increasing yield strength to approximately 1170 MPa and hardness to approximately 40–47 HRC while maintaining useful corrosion resistance. Compared with annealed AISI 321, 17-4 PH H900 offers substantially higher hardness and fatigue strength, which is expected to reduce the susceptibility to adhesive wear/galling and to increase the structural safety margin. The properties of 17-4 PH H900 are included in Table 3. To guarantee a rigorous and unbiased comparison, the validation simulation was executed using exactly the same geometric model, boundary conditions, load magnitude, and meshing strategy as in the diagnostic analysis of the AISI 321 plunger. The only altered variable was the material definition, allowing for a direct and unambiguous comparison of structural performance. This comparative methodology isolates the effect of material substitution on the component's mechanical integrity.

Table 3. Mechanical and physical properties.

Property	AISI 321 (Annealed)	17-4 PH H900
Yield strength, S_y	205 MPa	1170 MPa
Ultimate tensile strength, S_{ut}	515 MPa	1310 MPa
Young's modulus, E	193 GPa	196 GPa
Poisson's ratio, ν	0.29	0.25
Hardness	≤187 HB (typically 160–180 HB)	~40–47 HRC (~44 HRC)
Density	~7.93 g/cm^3	~7.80 g/cm^3
Thermal conductivity at 20 °C	~16.0 W/(m·K)	~18 W/(m·K)
Specific heat at 20 °C	~500 J/(kg·K)	~460 J/(kg·K)

2.4. Manufacturing Technology

The manufacturing protocol for the proposed 17-4 PH plunger was designed to be technologically robust and adapted to the resources available at the thermoelectric plant, including a conventional 16K20 model lathe. The central strategy consisted of performing all chip-removal machining operations on the material in its solution-annealed state (Condition A), which presents optimal machinability. Subsequently, the part undergoes heat treatment to achieve the final hardness and strength, concluding with a precision finishing operation. The turning operations sequence was defined to ensure the part's dimensional accuracy and concentricity. The general process flow is summarized in the diagram in Figure 5. Starting from a calibrated Ø14 mm bar, sequential operations included facing, center drilling for between-centers mounting, rough turning for the various diameters, and finally, threading and chamfering. To ensure process efficiency, cutting regimes were calculated for each operation. As a representative example, for the main rough turning operation (from Ø14 to Ø10.5 mm), a CNMG 120,408 MM (Grade GC 2025) cemented carbide insert was selected. The cutting parameters calculated for this operation were a depth of cut (t) of 1.75 mm, a feed rate (f) of 0.25 mm/rev, and a spindle speed (n) of 1600 rpm, resulting in an effective cutting speed (Vc) of 70.4 m/min [29].

Following the primary machining stages, the component is subjected to a precipitation hardening (aging) heat treatment to transform it from Condition A to the target H900 condition. This thermal cycle, represented in Figure 6, consists of heating the component to 482 °C (900 °F) and holding it at this temperature for 60 min, followed by air cooling. This process generates a fine dispersion of copper-rich precipitates within the martensitic matrix, which is responsible for the significant increase in hardness and yield strength.

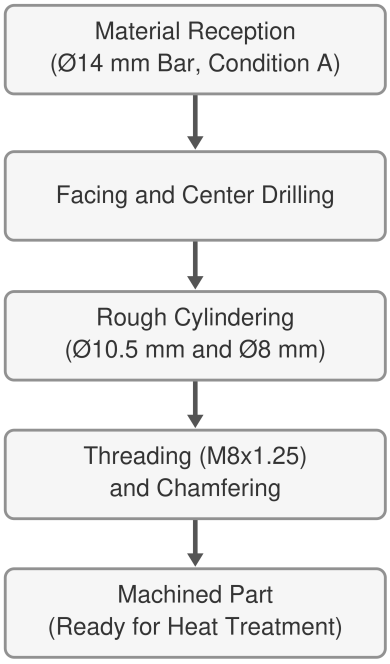


Figure 5. A simplified flowchart of the turning operations sequence for the manufacture of the proposed plunger.

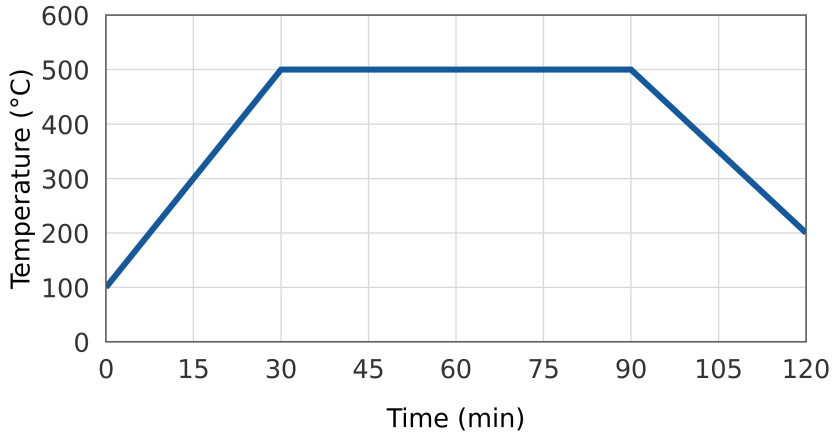


Figure 6. Aging heat treatment cycle to achieve the H900 condition in 17-4 PH stainless steel, specifying temperature and time parameters.

The final manufacturing step is a cylindrical grinding operation performed on the main working surface of the plunger (the Ø10 mm diameter). This precision finishing process is critical to achieving the final dimensional tolerances and the required surface finish ($Ra \leqslant 0.8$ μm). Low surface roughness is essential to minimize friction and prevent the initiation of wear mechanisms, thereby ensuring the long-term tribological performance of the component.

3. Results

This section presents the quantitative findings derived from the finite element analyses (FEAs). The results are presented sequentially: first, the diagnosis of the original plunger to establish a baseline of the problem; second, the validation of the redesigned plunger to demonstrate its structural superiority; and finally, a comparative synthesis summarizing the key improvements.

3.1. Structural Analysis of the Original Plunger (AISI 321)

At the maximum operating pressure of 25 MPa, the original AISI 321 plunger reaches a maximum von Mises stress of 199.4 MPa, corresponding to approximately 97.3% of the nominal yield strength and a safety factor of only 1.03. This result should be interpreted as evidence of an extremely limited structural reserve rather than direct proof of plastic deformation. Under the linear-elastic assumptions of the present model, the estimated pressure corresponding to the onset of yielding would be approximately 25.8 MPa, only about 3% above the nominal maximum operating pressure. Consequently, relatively small pressure transients, dimensional tolerances, residual stresses, or variations in material strength could promote localized yielding during service. Such permanent deformation may subsequently modify alignment and contact-pressure distribution at the plunger–guide interface, providing a plausible indirect mechanism for accelerating galling. Nevertheless, this coupling remains a mechanistic hypothesis that should be further validated through cyclic elastoplastic and explicit contact analyses. Figure 7 presents a composite visualization of these critical results. It shows how the area of maximum stress coincides directly with the zone of minimum safety factor, confirming that the original design is structurally deficient.

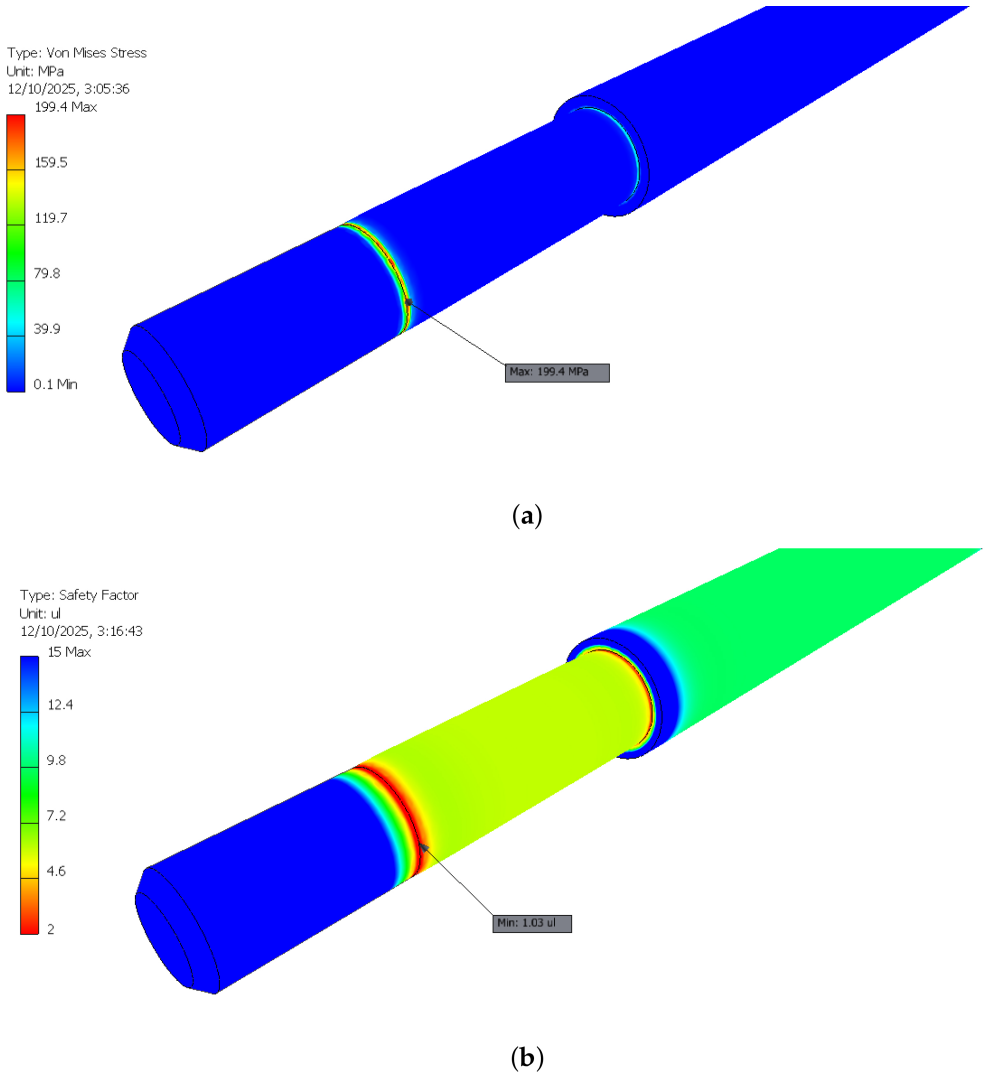


Figure 7. Structural analysis of the original AISI 321 plunger. (**a**) Von Mises Stress distribution, showing a maximum value of 199.4 MPa concentrated at the cross-section change. (**b**) Safety factor distribution, revealing a critical zone with a minimum value of 1.03. The color scale in (**b**) is adjusted to highlight areas with SF $\leqslant$ 1.5 in red.

Deformation Analysis: The maximum total resultant displacement was 0.02644 mm, located at the center of the front face of the plunger, where the pressure is applied. This deformation, being of an extremely small magnitude relative to the overall dimensions of the plunger (length and diameter), allows us to rule out macroscopic buckling or significant lateral bending ("deflection") as the primary failure mode. The component exhibits high axial stiffness, but its design is inadequate from a material strength perspective.

3.2. Structural Validation of the Redesigned Plunger (17-4 PH H900)

The comparative analysis of the redesigned plunger, using the 17-4 PH material in the H900 condition and under the same boundary and loading conditions, demonstrated a substantial improvement in structural integrity.

Stress State and Safety Factor: The maximum von Mises stress in the new design was 203.7 MPa, a value similar to that of the original design and located in the same geometric region. However, when contrasting this stress with the high yield strength of 17-4 PH H900 (Sy= 1170 MPa), the working stress represents only 17.4% of the material's capacity. This wide margin translates into a minimum safety factor of 5.74, as clearly illustrated in Figure 8. This result confirms that the new design operates safely within the elastic regime, eliminating the risk of micro-plastic deformations that accelerate galling wear.

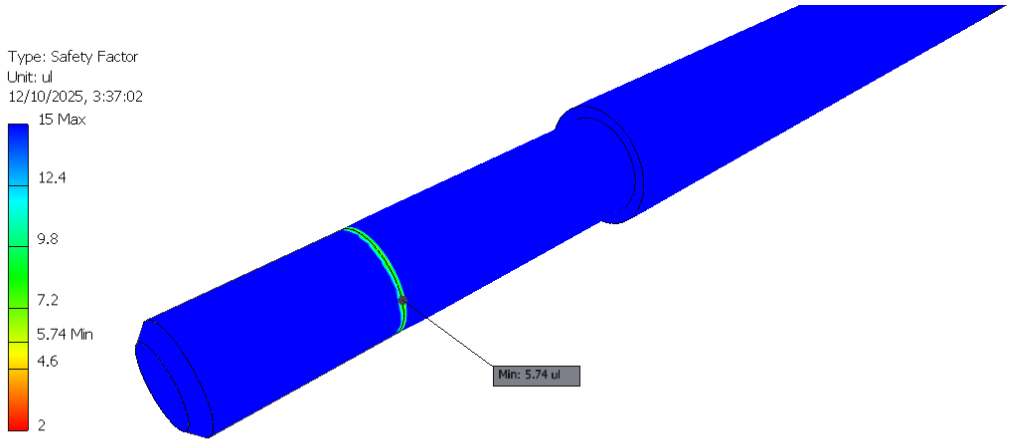


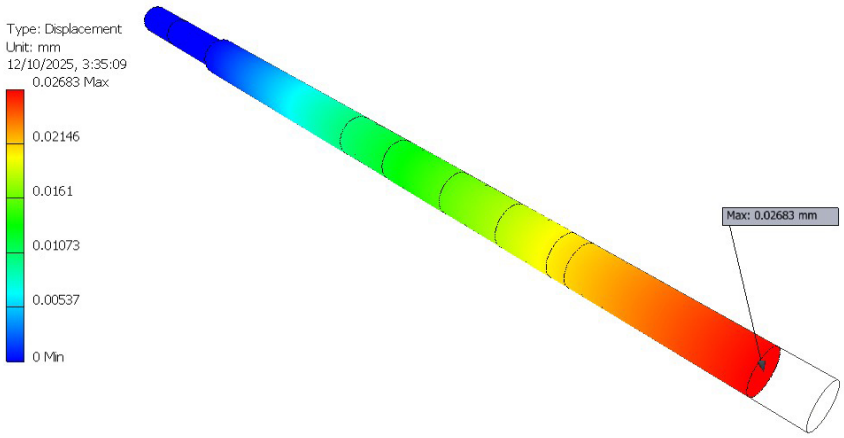
Figure 8. The safety factor distribution for the redesigned 17-4 PH H900 plunger. The minimum value is 5.74, indicating a structurally robust design. For direct visual comparison, the same color scale as in Figure 4b has been maintained, showing no low safety-factor zones.

Deformation and Principal Stress Analysis: The proposed plunger exhibited a maximum total displacement of 0.02683 mm, as shown in Figure 9a. This value is practically identical to that of the original plunger, indicating comparable stiffness under the evaluated loading and boundary conditions. Figure 9b presents the third principal stress distribution, with values ranging from −223.1 to 0.7 MPa. The minimum value identifies the region subjected to the greatest compressive principal stress. Together, these results characterize the deformation and compressive stress response of the proposed design.

3.3. Comparative Synthesis of Results

To facilitate a direct performance evaluation, Table 4 summarizes the key mechanical performance indicators for both designs. The analysis evidences that, while the stress and deformation profiles are comparable due to the identical geometry and similar elastic moduli, the improvement in the safety factor is the critical differentiator. The proposed

solution offers a 457% increase in the structural safety margin, transforming a deficient design into a robust and reliable one.



(**a**)



(**b**)

Figure 9. The finite element results for the proposed 17-4 PH H900 plunger: (**a**) total displacement distribution, with a maximum value of 0.02683 mm at the front face, and (**b**) third principal stress distribution, ranging from −223.1 to 0.7 MPa.

Table 4. Performance comparison between original and proposed plungers.

Performance Parameter	Original Plunger (AISI 321)	Proposed Plunger (17-4 PH H900)	Improvement (%)
Maximum von Mises Stress (MPa)	199.4	203.7	N/A *
Maximum Displacement (mm)	0.02644	0.02683	N/A *
Minimum Safety Factor	1.03	5.74	+457%

* The improvement is not applicable (N/A) as the values are of similar magnitude; the key performance indicator is the increase in the safety factor.

3.4. Techno-Economic Feasibility via Life-Cycle Cost (LCC) Analysis

A techno-economic feasibility analysis was conducted to compare the current strategy, based on importing the original plunger (AISI 321), with the proposed strategy of locally manufacturing a redesigned and optimized plunger (17-4 PH H900). For this purpose, the Life-Cycle Cost (LCC) analysis methodology was applied, a standardized approach that

evaluates the total cost of ownership of an asset, rather than focusing solely on its initial acquisition cost. This method is particularly suitable for quantifying the long-term benefits of investments in components with higher reliability and durability [30,31]. The analysis compares two scenarios:

- Scenario A (Baseline): Importation of the original spare part. This strategy is characterized by an acquisition cost that includes not only the component's price but also significant logistics costs, tariffs, and, critically, long and uncertain lead times.
- Scenario B (Proposal): Local manufacturing of the redesigned plunger. This strategy implies a potentially higher initial manufacturing cost but offers immediate spare part availability and a drastically extended service life.

For the comparison, costs were normalized by taking the acquisition cost of the imported spare part as the base cost unit (1.0). The key parameters of the analysis are summarized in Table 5. The estimation of a 30% higher acquisition cost (Cadq = 1.3) for the locally manufactured plunger is a conservative projection that considers the higher value of the 17-4 PH steel and the heat treatment process. Similarly, a relative service life of 10.0 (V_u = 10.0) was considered as a favorable long-term performance scenario for the proposed component. This value should not be interpreted as a direct prediction of service life, since experimental field validation of the redesigned plunger has not yet been performed. Instead, it represents an upper-bound scenario used to explore the potential economic benefits associated with the improved structural margin and higher hardness of 17-4 PH H900. Finally, the zero lead time of local manufacturing drastically reduces the economic impact of plant downtime (C_parada), a factor exacerbated by the long waiting times associated with importation [32].

Table 5. Comparative parameters for the LCC analysis of maintenance strategies.

Parameter	Scenario A: Importation (AISI 321)	Scenario B: Local Manufacturing (17-4 PH)
Normalized Acquisition Cost (Cadq)	1.0 (Baseline)	1.3
Relative Service Life (Vu)	1.0	10.0
Lead Time	High (Weeks/Months)	Zero
Downtime Cost (Cparada)	Cparada (magnified by lead time)	Cparada (minimized to replacement time)

The normalized total cost of wwnership for an operating cycle equivalent to the proposed plunger's service life (10 life units) is calculated as follows:

$$\text{Total Cost (Scenario A)} = 10 \times (C_{\text{adq imported}} + C_{\text{extended downtime}}) = 10.0 + 10\,C_{\text{extended downtime}} \quad (1)$$

$$\text{Total Cost (Scenario B)} = 1 \times (C_{\text{adq local}} + C_{\text{minimal downtime}}) = 1.3 + 1\,C_{\text{minimal downtime}} \quad (2)$$

To reduce the dependence of the economic assessment on the assumed tenfold service-life scenario, the normalized replacement cost per unit of service life was additionally expressed as

$$C_{\text{rel}} = \frac{C_{\text{local}}}{L_r}, \quad (3)$$

where $C_{\text{local}} = 1.3$ is the normalized acquisition cost of the locally manufactured component and L_r is its service life relative to that of the original plunger. The break-even condition is obtained when $C_{\text{rel}} = 1$:

$$\frac{1.3}{L_r} = 1, \quad (4)$$

which gives

$$L_r = 1.3. \quad (5)$$

Considering the four-month service life observed for the original AISI 321 plunger, the minimum service life required for the proposed component to reach the break-even point is

$$L_{\text{break-even}} = 4(1.3) = 5.2 \text{ months.} \quad (6)$$

The relative service life of 10.0 used in the LCC analysis is a design assumption based on the material property improvements of 17-4 PH H900 relative to the original annealed AISI 321. It is not a break-even value and should not be interpreted as a prediction or as a minimum economic threshold. The original plunger failed after approximately four months of service. The redesigned component is expected to operate for multiple years, as supported by the following quantitative improvements: yield strength increases from 205 MPa to 1170 MPa (5.7×), hardness increases from approximately 85 HRB to 40–47 HRC (>2.5× on an equivalent scale), corrected fatigue limit increases from approximately 128.5 MPa to approximately 316 MPa (2.5× under the same correction factors), and minimum safety factor increases from 1.03 to 5.74 (a 457% improvement). These improvements directly address the two identified failure mechanisms: localized yielding due to insufficient structural reserve and adhesive wear/galling due to low surface hardness. Therefore, a tenfold increase in service life (approximately 40 months, or more than three years) is a conservative lower-bound estimate of the expected multi-year performance, not an optimistic upper-bound scenario. The actual service life must be confirmed through controlled field trials.

To reduce the uncertainty associated with the assumed service-life extension of the redesigned plunger, the economic assessment was complemented by a sensitivity analysis based on relative durability. As shown in Figure 10, the normalized cost per unit of service life decreases progressively as the operational life of the locally manufactured 17-4 PH H900 plunger increases relative to that of the original AISI 321 component. The reference condition $C_{\text{rel}} = 1$ defines the break-even threshold, thereby providing a direct criterion for determining the minimum durability improvement required to offset the higher initial manufacturing cost. This representation demonstrates that the economic feasibility of the proposed strategy can be assessed independently of the assumed tenfold life-extension scenario.

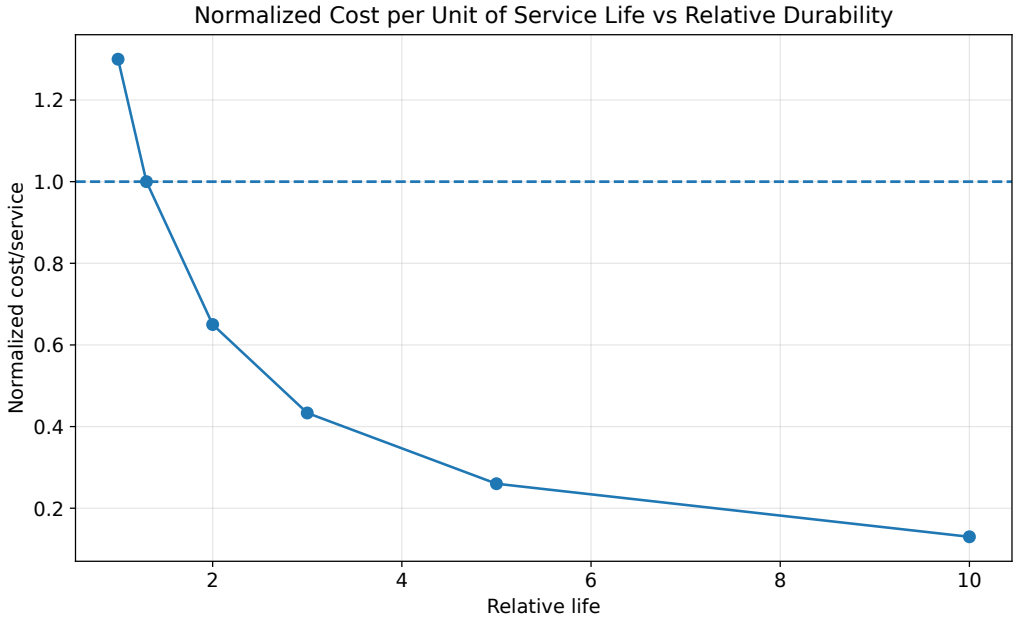


Figure 10. Normalized cost per unit of service life as a function of the relative durability of the locally manufactured 17-4 PH H900 plunger. The horizontal dashed line at $C_{\text{rel}} = 1$ represents the economic break-even condition relative to the imported AISI 321 component.

4. Discussion

The results obtained in this study provide a mechanistic interpretation of the premature degradation observed in the AISI 321 dosing pump plunger and support the evaluation of the structural advantages associated with the proposed 17-4 PH H900 replacement. The numerical analysis indicates that the original component operates with a critically limited structural safety margin while simultaneously being exposed to unfavorable tribological conditions that promote galling. However, since the present finite element model is based on a linear-elastic formulation and does not explicitly account for cyclic plasticity, frictional contact, or wear evolution, the interaction between the structural response and the observed galling should be interpreted as a mechanically plausible tribo-mechanical coupling rather than as a directly demonstrated causal sequence. Accordingly, the discussion focuses on the extent to which the structural deficiency may contribute to the degradation of the contact conditions and on the capacity of the proposed material substitution to increase the mechanical robustness of the component.

4.1. Elucidation of a Systemic Failure: Indirect Interaction Between Structural and Tribological Deficiencies

The primary finding of this research is that the plunger's premature failure cannot be attributed to a single cause but rather to a systemically deficient design with critical structural and tribological vulnerabilities.

The finite element analysis (Figure 7) identified a severe stress concentration at the cross-section change near the thread, where the von Mises stress reached 199.4 MPa, equivalent to 97.3% of the AISI 321's yield strength. This finding is irrefutable evidence of a structural design deficiency that pushed the component to the brink of localized plastic yielding, with a critical safety factor of 1.03.

Although this maximum stress point does not spatially coincide with the working surface (Ø10 mm) where galling occurs, both problems are intrinsically linked. The structural deficiency and the tribological failure are concurrent manifestations of inadequate material selection and design philosophy for the application. However, an indirect coupling mechanism that accelerates failure is postulated:

1. Initiation of Micro-Plastic Deformation: The cyclic stress at the stress concentrator, being so close to the yield point, induces cumulative micro-plastic deformations. Over time, this ratcheting phenomenon can compromise the nanometric straightness of the plunger.
2. Degradation of Guide Contact: A minimal deviation in straightness fundamentally alters the contact pressure distribution between the plunger and the guides. Instead of uniform contact, edge loading is generated, with localized pressure peaks far exceeding nominal values.
3. Acceleration of Galling: These localized pressure peaks are a known catalyst for adhesive wear, as they effectively break the protective passive layer of the stainless steel, initiating the destructive cycle of adhesion and material tear-out that defines galling.

Therefore, it is concluded that the failure is of a tribo-mechanical nature, but the interaction is indirect. The structural deficiency not only represents an independent failure mode but also acts as an accelerator of wear by degrading the contact conditions at the tribological interface. The successful redesign, therefore, had to address both deficiencies simultaneously.

4.2. Rationalization of the Redesign: Toward Robust Engineering

The effectiveness of the proposed solution lies in its comprehensive approach to mitigating both the mechanical cause and the tribological effect. The selection of 17-4 PH stainless steel in the H900 condition is justified through a multi-factorial analysis, as illustrated in the material performance map in Figure 11.

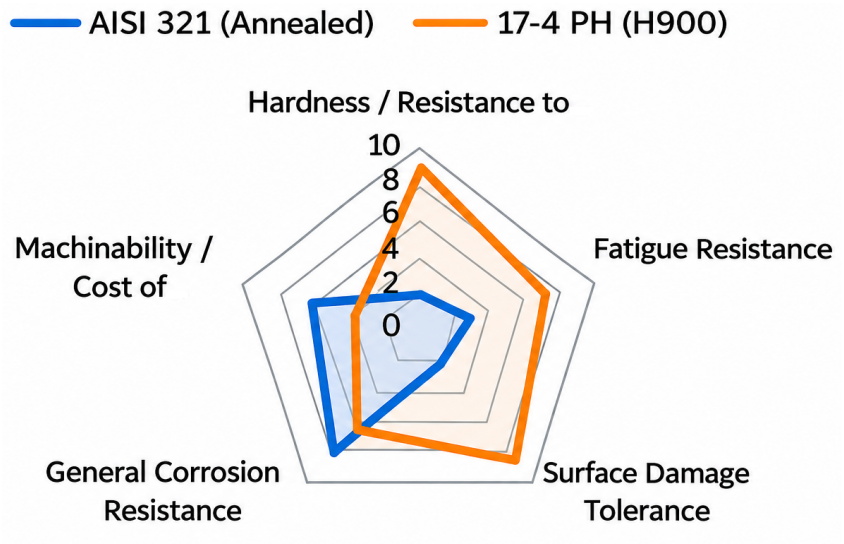


Figure 11. Comparative material performance map. The chart represents a semi-quantitative evaluation based on established material properties from the technical literature and engineering handbooks. The 17-4 PH (H900) shows an overwhelming superiority in critical properties for this application—hardness/wear resistance and fatigue strength—while maintaining excellent corrosion resistance. The only trade-off is lower machinability, which translates into a moderately higher manufacturing cost.

The map in Figure 11 evidences a clear design trade-off. The use of 17-4 PH steel for applications demanding high wear and fatigue resistance is well documented in engineering handbooks and is common in valve and pump components for the chemical industry; however, this study validates its suitability for this specific application [33,34]. While AISI 321 presents better machinability, 17-4 PH H900 drastically outperforms it in the two properties that directly attack the failure mechanism: hardness, which intrinsically inhibits adhesion and wear, and fatigue strength (closely tied to yield strength), which is the property that resolves the structural deficiency. The FEA validates this selection quantitatively. By raising the safety factor to 5.74, the new design not only prevents failure from overload but also shifts the component's operating point to a low-stress regime (only 17.4% of its yield strength). This enormous safety margin should not be interpreted as over-engineering but as a pillar of robust design, necessary to absorb unforeseen pressure peaks, material imperfections, and the natural degradation of properties over time, thereby guaranteeing reliability in a demanding industrial environment.

To critically assess the suitability of the proposed material substitution, Table 6 compares the principal mechanical, tribological, and manufacturing characteristics of AISI 321 and 17-4 PH H900 stainless steels. The comparison highlights that the main advantage of 17-4 PH H900 is not associated with a significant change in elastic stiffness, but with its substantially higher yield strength and hardness, which increase the structural reserve and may reduce susceptibility to localized plastic deformation and adhesive wear. At the same time, the selection introduces additional considerations related to heat treatment, machining, and environment-dependent corrosion performance. Therefore, the material substitution represents a balance between improved mechanical robustness and

increased manufacturing requirements rather than an unequivocal improvement in all material attributes.

Table 6. Comparison of material-selection criteria for the original AISI 321 plunger and the proposed 17-4 PH H900 configuration.

Property	AISI 321	17-4 PH H900	Engineering Relevance
Yield strength [35]	205 MPa	1170 MPa	Resistance to localized yielding and increased structural reserve
Young's modulus [11]	193 GPa	196 GPa	Elastic stiffness and dimensional response under load
Relative hardness [36]	Lower	Higher	Resistance to localized plastic deformation and adhesive wear
Corrosion resistance [37]	Generally high	High, but dependent on aging condition and environment *	Compatibility with the service medium and preservation of surface integrity
Heat-treatment condition [38]	Annealed	H900 aging	Development of strength and hardness through precipitation hardening
Manufacturing considerations [39]	Conventional machining; susceptible to work hardening	Machining in Condition A followed by H900 aging and final grinding	Manufacturing complexity and preservation of dimensional accuracy
Structural safety factor [40]	1.03	5.74	Structural reliability under the maximum operating pressure

* The corrosion performance of 17-4 PH stainless steel depends on the heat-treatment condition and environmental exposure and should therefore be experimentally verified for the specific service medium.

4.3. Implications of the Study and Contribution

The implications of this work extend beyond solving a specific maintenance problem in a thermoelectric plant. Industrial and Practical Implications: The main practical contribution is the provision of a complete engineering solution—design, material, and manufacturing technology—that allows the substitution of a failure-prone imported spare part with a local component of superior reliability. This not only solves a chronic operational problem and reduces costly unscheduled downtime but also sets a precedent for technological sovereignty in critical asset management. Methodological Implications: This study presents a systematic and transferable framework for forensic engineering and component redesign. The sequence of (1) root cause diagnosis via realistic FEA, (2) materials science-based redesign, (3) comparative numerical validation, and (4) feasibility analysis via LCC, constitutes a robust "roadmap" that can be applied to solve a wide range of failures in industrial machinery.

4.4. Limitations and Future Research Directions

It is imperative to acknowledge the limitations of this study to maintain scientific rigor. The research is based on numerical analysis, which, although performed with high fidelity, involves certain idealizations. The main limitations are (1) the use of a static analysis, which represents the worst loading case but does not model the cumulative effects of fatigue over millions of cycles; (2) the idealization of boundary conditions, such as the frictionless support; and (3) the absence of experimental validation of the final component. These limitations clearly outline directions for future research. The logical and highest-priority next step is the manufacturing of a prototype of the redesigned plunger and its installation in the dosing pump for a long-term field test. This would allow experimental validation of the predictions of this study and quantification of the actual extension of service life. Additionally, future numerical work could include a fatigue analysis to predict the number of cycles to failure and explore topological optimizations to reduce the weight and cost of the component without compromising its structural robustness.

5. Conclusions

The finite element analysis of the original AISI 321 plunger under the maximum operating pressure of 25 MPa revealed a maximum von Mises stress of 199.4 MPa and a

minimum safety factor of 1.03. This indicates an extremely limited structural reserve, with the estimated yield onset pressure only about 3% above the nominal operating pressure. Such a condition makes the component susceptible to localized yielding under pressure transients, dimensional tolerances, or material variability. The observed galling damage is interpreted as a failure in which the structural deficiency may have indirectly contributed to adhesive wear by altering the contact conditions at the plunger–guide interface. This coupling remains a mechanistic hypothesis supported by visual evidence and the literature, and it was not experimentally validated in the present study.

Under identical FEA conditions, the redesigned plunger manufactured from 17-4 PH stainless steel in the H900 condition exhibited a maximum von Mises stress of 203.7 MPa, which corresponds to only 17.4% of its yield strength. The minimum safety factor increased to 5.74, representing a 457% improvement in the structural safety margin relative to the original design. The maximum displacement remained practically unchanged at 0.02683 mm, confirming that the higher-strength material does not compromise the component's axial stiffness. The H900 condition, achieved by aging at 482 °C for 1 h followed by air cooling, provides a hardness of approximately 40–47 HRC and a yield strength of about 1170 MPa, which directly addresses both the structural deficiency and the susceptibility to adhesive wear.

A feasible local manufacturing route was defined, consisting of turning in the solution-annealed Condition A, precipitation hardening to H900, and cylindrical grinding of the working diameter to $R_a \leq 0.8$ μm. The combination of higher hardness, higher fatigue strength, and a substantially increased safety factor is expected to improve the durability of the plunger relative to the four-month baseline observed for the original component, although the actual service life must be confirmed through controlled field trials. These improvements are based on the 5.7× increase in yield strength, the >2.5× increase in hardness, and the 2.5× increase in corrected fatigue limit of 17-4 PH H900 relative to annealed AISI 321. The Life-Cycle Cost analysis indicated the economic superiority of local manufacturing over importing the original spare part. The break-even analysis indicated that local manufacturing becomes economically advantageous even for service-life improvements well below the values assumed in the present study. The actual economic benefit will depend on the service life achieved in practice, which remains to be experimentally verified.

The main limitations of this study are the use of a static linear-elastic FEA, idealized boundary conditions, and the absence of experimental tribological and field validation. Future work should include cyclic elastoplastic and explicit contact analyses, tribological testing, and a controlled field trial to confirm the expected service life and to quantify the actual reduction in galling susceptibility.

Author Contributions: Conceptualization, D.d.A.Y., C.L.R.V., C.D.C.-R. and J.R.-R.; methodology, Y.C.A., L.A.I.C. and J.R.-R.; software, D.d.A.Y. and C.D.C.-R.; validation, D.d.A.Y., C.L.R.V. and L.A.I.C.; formal analysis, D.d.A.Y., C.L.R.V. and Y.C.A.; investigation, D.d.A.Y., C.L.R.V., Y.C.A., L.A.I.C. and J.R.-R.; resources, C.D.C.-R., L.A.I.C. and J.R.-R.; data curation, L.A.I.C., C.L.R.V., Y.C.A. and J.R.-R.; writing—original draft preparation, D.d.A.Y., Y.C.A. and C.D.C.-R.; writing—review and editing, C.D.C.-R., Y.C.A. and J.R.-R.; project administration, C.D.C.-R. and L.A.I.C.; funding acquisition, C.D.C.-R., L.A.I.C. and J.R.-R. All authors have read and agreed to the published version of the manuscript.

Funding: This research received no external funding.

Institutional Review Board Statement: Not applicable.

Informed Consent Statement: Not applicable.

Data Availability Statement: The data presented in this study, including 3D CAD models and finite element simulation files, are available on request from the corresponding authors. The data are not publicly available due to their proprietary nature related to the power plant's critical infrastructure.

Acknowledgments: The authors would like to express their profound gratitude to the technical and administrative staff at the "Carlos Manuel de Céspedes" Thermoelectric Power Plant in Cienfuegos, Cuba, for their invaluable support. Special thanks to for facilitating access to the facilities, providing operational data, and assisting during the diagnosis of the failed components.

Conflicts of Interest: The authors declare no conflicts of interest.

References

1. Petrova, T.I.; Orlov, K.A.; Dooley, R.B. International water and steam quality standards for thermal power station drum-type and waste heat recovery boilers with the treatment of boiler water with phosphates and NaOH. *Therm. Eng.* **2017**, *64*, 61–67. [CrossRef]
2. Tuz, V.; Kravets, V.; Lebed, N.; Vorobiov, M. Prediction of Onset of Boiling Conditions in Steam-Generating Elements of Natural Circulation Power Units. *Energy Technol. Resour. Sav.* **2026**, *86*, 85–93. [CrossRef]
3. Dooley, R.; McNaughton, W. *Boiler and Heat Recovery Steam Generator Tube Failures: Theory and Practice, Volume 1: Fundamentals*; Technical Report Report 1012757; Electric Power Research Institute (EPRI): Palo Alto, CA, USA, 2007.
4. Wilcox, B. *Steam: Its Generation and Use*, 41st ed.; The Babcock & Wilcox Company: Barberton, OH, USA, 2005.
5. Kóti, D.; Daure, J.; Neate, N.; Stewart, D.; Shipway, P. Characterisation of damage in galling testing of austenitic stainless steel as a function of pressure and sliding distance. *Wear* **2025**, *571*, 205776. [CrossRef]
6. Ding, L.; Li, Y. Reduction of Friction and Wear for AISI321 Stainless Steel through Surface Modification Using Nanocrystallization. *Materials* **2023**, *16*, 5303. [CrossRef]
7. Macknojia, A.Z.; Montoya, V.L.; Cairns, E.; Eskandari, M.; Liu, S.; Chung, Y.W.; Wang, Q.J.; Berkebile, S.P.; Aouadi, S.M.; Voevodin, A.A.; et al. Tribological Analysis of Steels in Fuel Environments: Impact of Alloy Content and Hardness. *Appl. Sci.* **2024**, *14*, 1898. [CrossRef]
8. Kharlamov, Y.; Sokolov, V.; Krol, O.; Romanchenko, O. Experimental Research of the Tribological Properties of D-Gun Sprayed WC – Co Coatings. In *Innovations in Mechanical Engineering*; Machado, J., Soares, F., Trojanowska, J., Ottaviano, E., Eds.; Springer: Cham, Switzerland, 2022; pp. 34–45. [CrossRef]
9. Savrai, R.; Skorynina, P. Structural-phase transformations and changes in the properties of AISI 321 stainless steel induced by liquid carburizing at low temperature. *Surf. Coat. Technol.* **2022**, *443*, 128613. [CrossRef]
10. Chen, Y.; Xu, B.; Liu, Y.; Liang, X.; Xu, Y. Structure and sliding wear behavior of 321 stainless steel/Al composite coating deposited by high velocity arc spraying technique. *Trans. Nonferrous Met. Soc. China* **2008**, *18*, 603–609. [CrossRef]
11. Yu, L.; Xiao, C.; Jiang, W.; Li, W.; Ni, S.; Song, M. Effects of aluminizing on the microstructure and wear resistance of AISI 321 steel. *Surf. Coat. Technol.* **2024**, *483*, 130753. [CrossRef]
12. Qin, W.; Kang, J.; Li, J.; Yue, W.; Liu, Y.; She, D.; Mao, Q.; Li, Y. Tribological Behavior of the 316L Stainless Steel with Heterogeneous Lamella Structure. *Materials* **2018**, *11*, 1839. [CrossRef]
13. Jourani, A.; Bouvier, S. Friction and Wear Mechanisms of 316L Stainless Steel in Dry Sliding Contact: Effect of Abrasive Particle Size. *Tribol. Trans.* **2015**, *58*, 131–139. [CrossRef]
14. Gåård, A.; Hallbäck, N.; Krakhmalev, P.; Bergström, J. Temperature effects on adhesive wear in dry sliding contacts. *Wear* **2010**, *268*, 968–975. [CrossRef]
15. Lin, N.; Liu, Q.; Zou, J.; Guo, J.; Li, D.; Yuan, S.; Ma, Y.; Wang, Z.; Wang, Z.; Tang, B. Surface Texturing-Plasma Nitriding Duplex Treatment for Improving Tribological Performance of AISI 316 Stainless Steel. *Materials* **2016**, *9*, 875. [CrossRef]
16. Podgornik, B. Adhesive Wear Failures. *J. Fail. Anal. Prev.* **2022**, *22*, 113–138. [CrossRef]
17. Yang, X.; Liu, H.; Zhang, L.; Hu, Y.; Politis, D.J.; Gharbi, M.M.; Wang, L. Interactive mechanism and friction modelling of transient tribological phenomena in metal forming processes: A review. *Friction* **2024**, *12*, 375–395. [CrossRef]
18. Gerritsen, S.; Bauer, A. S^3P– Innovative Surface Treatment to Increase the Wear Resistance of Stainless Steel Components. *HTM J. Heat Treat. Mater.* **2022**, *77*, 425–436. [CrossRef]
19. Zawadzki, P.; Dobrotvorskiy, S.; Aleksenko, B.; Talar, R. Effect of Nanosecond Laser Texturization on Tribological Behavior of AISI 321 Stainless Steel. *Materials* **2024**, *17*, 5870. [CrossRef]
20. Borgioli, F. The Corrosion Behavior in Different Environments of Austenitic Stainless Steels Subjected to Thermochemical Surface Treatments at Low Temperatures: An Overview. *Metals* **2023**, *13*, 776. [CrossRef]
21. Xiao, N.; Tang, J.; Zhou, S.; Shi, Y.; Qian, F.; Qiu, S.; Chen, Y.; Zhao, D.; Yang, K. Current research on the design, properties and applications of tribological materials: A review. *RSC Adv.* **2025**, *15*, 34669–34717. [CrossRef]

22. Yang, X.; Lei, J.; Bi, Y.; Yu, M.; Yi, Y. Torsional fatigue failure study and lightweight design of hybrid engine crankshaft based on multidimensional analysis and experimental-simulation synergy. *Eng. Fail. Anal.* **2025**, *182*, 110145. [CrossRef]
23. Koleda, E.V.; Kireev, S.O.; Korchagina, M.V.; Efimov, A.V.; Sperling, J. Strength Analysis of the TWS 600 Plunger Pump Body in SolidWorks Simulation. *Adv. Eng. Res.* **2021**, *21*, 71–81. [CrossRef]
24. Autodesk, Inc. *Autodesk Inventor Professional 2025*; Autodesk, Inc.: San Francisco, CA, USA, 2024.
25. ASM International. *ASM Handbook, Volume 1: Properties and Selection: Irons, Steels, and High-Performance Alloys*; ASM International: Materials Park, OH, USA, 1990.
26. Smallman, R.; Ngan, A. *Modern Physical Metallurgy*, 8th ed.; Butterworth-Heinemann: Oxford, UK, 2007.
27. HAOSH Pumps. *Technical Data Sheet*; HAOSH Pumps: Shanghai, China, 2024.
28. Reddy, J. *An Introduction to the Finite Element Method*, 4th ed.; McGraw-Hill Education: New York, NY, USA, 2019.
29. Dobrovolski, V.; Zablonski, K.; Mak, S.; Radchik, A.; Erlikh, L. *Machine Elements: A Textbook*; Mir Publishers: Moscow, Russia, 1984.
30. *ISO 15686-5:2017*; Buildings and Constructed Assets—Service Life Planning—Part 5: Life-Cycle Costing. International Organization for Standardization: Geneva, Switzerland, 2017.
31. Dhillon, B. *Life Cycle Costing for Engineers*; CRC Press: Boca Raton, FL, USA, 2010.
32. Blanchard, B.; Fabrycky, W. *Systems Engineering and Analysis*, 5th ed.; Prentice Hall: Upper Saddle River, NJ, USA, 2011.
33. Davis, J. (Ed.) *Stainless Steels*; ASM International: Materials Park, OH, USA, 1999.
34. Mills, G. *Materials for Valves*; Elsevier: Amsterdam, The Netherlands, 2002.
35. Bressan, J.; Daros, D.; Sokolowski, A.; Mesquita, R.; Barbosa, C. Influence of hardness on the wear resistance of 17-4 PH stainless steel evaluated by the pin-on-disc testing. *J. Mater. Process. Technol.* **2008**, *205*, 353–359. [CrossRef]
36. Tai, S.; Lee, I.K.; Lin, M.Y.; Liao, K.Y.; Chang, C.C.; Lee, H.B. Effect of Heat Treatment on the Corrosion and Wear Behavior of 17-4 PH Stainless Steel for Marine Applications. *J. Mar. Sci. Technol.* **2026**, *34*, 5.
37. Cho, Y.H.; Park, S.Y.; Kim, J.Y.; Yun, J.Y.; Lee, K.A. Effect of heat treatment on microstructure and corrosion behavior of 17-4 PH stainless steel fabricated via metal material extrusion additive manufacturing. *J. Mater. Res. Technol.* **2025**, *38*, 3524–3546. [CrossRef]
38. Pasebani, S.; Ghayoor, M.; Badwe, S.; Irrinki, H.; Atre, S.V. Effects of atomizing media and post processing on mechanical properties of 17-4 PH stainless steel manufactured via selective laser melting. *Addit. Manuf.* **2018**, *22*, 127–137. [CrossRef]
39. Robles, A.; Astarloa, A.; Llanos, I.; Mancisidor, I.; Fernandes, M.H.; Munoa, J. Comparison of Modulation-Assisted Machining Strategies for Achieving Chip Breakage When Turning 17-4 PH Stainless Steel. *J. Manuf. Mater. Process.* **2024**, *8*, 167. [CrossRef]
40. Leksycki, K.; Feldshtein, E.; Lisowicz, J.; Chudy, R.; Mrugalski, R. Cutting Forces and Chip Shaping When Finish Turning of 17-4 PH Stainless Steel under Dry, Wet, and MQL Machining Conditions. *Metals* **2020**, *10*, 1187. [CrossRef]

Disclaimer/Publisher's Note: The statements, opinions and data contained in all publications are solely those of the individual author(s) and contributor(s) and not of MDPI and/or the editor(s). MDPI and/or the editor(s) disclaim responsibility for any injury to people or property resulting from any ideas, methods, instructions or products referred to in the content.